



HAL
open science

Pulsed-CPT Cs-Ne microcell atomic clock with frequency stability below 2×10^{-12} at 105 s

Clément Carlé, Moustafa Abdel Hafiz, Shervin Keshavarzi, Rémy Vicarini,
Nicolas Passilly, Rodolphe Boudot

► **To cite this version:**

Clément Carlé, Moustafa Abdel Hafiz, Shervin Keshavarzi, Rémy Vicarini, Nicolas Passilly, et al.. Pulsed-CPT Cs-Ne microcell atomic clock with frequency stability below 2×10^{-12} at 105 s. Optics Express, 2023, 31 (5), pp.8160 - 8169. 10.1364/OE.483039 . hal-04154022

HAL Id: hal-04154022

<https://hal.science/hal-04154022>

Submitted on 6 Jul 2023

HAL is a multi-disciplinary open access archive for the deposit and dissemination of scientific research documents, whether they are published or not. The documents may come from teaching and research institutions in France or abroad, or from public or private research centers.

L'archive ouverte pluridisciplinaire **HAL**, est destinée au dépôt et à la diffusion de documents scientifiques de niveau recherche, publiés ou non, émanant des établissements d'enseignement et de recherche français ou étrangers, des laboratoires publics ou privés.

Pulsed-CPT Cs-Ne microcell atomic clock with frequency stability below 2×10^{-12} at 10^5 s

CLÉMENT CARLÉ,¹ MOUSTAFA ABDEL HAFIZ,¹ SHERVIN KESHAVARZI,¹ RÉMY VICARINI,¹ NICOLAS PASSILLY,¹ AND RODOLPHE BOUDOT^{1,*}

¹FEMTO-ST, CNRS, UFC, ENSMM, 26, rue de l'Épitaphe, 25030 Besançon, France

*rodolphe.boudot@femto-st.fr

Abstract: We report on the mid-term stability progress of a table-top coherent population trapping (CPT) microcell atomic clock, previously limited by light-shift effects and variations of the cell inner atmosphere. The light-shift contribution is now mitigated through the use of a pulsed symmetric auto-balanced Ramsey (SABR) interrogation technique, combined with setup temperature, laser power and microwave power stabilization. In addition, Ne buffer gas pressure variations in the cell are now greatly reduced through the use of a micro-fabricated cell built with low permeation alumino-silicate glass (ASG) windows. Combining these approaches, the clock Allan deviation is measured to be 1.4×10^{-12} at 10^5 s. This stability level at 1 day is competitive with best current microwave microcell-based atomic clocks.

© 2023 Optica Publishing Group under the terms of the [Optica Open Access Publishing Agreement](#)

1. Introduction

Microwave chip-scale atomic clocks (CSACs) [1–6] based on coherent population trapping (CPT) [7] have met a significant success by offering a typical fractional frequency stability of a few 10^{-11} at 1 day integration time, in a low size, weight and power (SWaP) budget. These clocks are now deployed in navigation and positioning systems, secure communications, underwater sensor networks and unmanned vehicles. However, mid- and long-term instabilities remain and are likely to be resulting from light-shift effects and/or cell inner atmosphere evolution.

In a CPT CSAC, light-shifts are induced by variations of the laser power, laser frequency and microwave power and result in variations of the clock frequency. Various techniques have been demonstrated in continuous-regime (CW) CPT clocks to mitigate them such as the active stabilization on a specific microwave power set-point [8–11], the adjustment of the cell temperature [12], the compensation of the laser frequency detuning [11], the use of servo loops to mitigate variations of the laser block [6, 11, 13, 14], or the implementation of laser power modulation-based sequences [15, 16].

An alternative approach for light-shift mitigation consists in using pulsed Ramsey-based interrogation protocols. Their benefit for the improvement of mid- and long-term stability of vapor cell clocks, a specification of key importance for most of the applications, has been demonstrated in high-performance double-resonance Rb cell clocks with the pulsed-optically pumped (POP) method [17] or CPT clocks using symmetric auto-balanced Ramsey spectroscopy (SABR) [18]. These pulsed cell clocks have demonstrated long-term stability levels never achieved by their continuous-regime (CW) version. More recently, these interrogation methods were adopted with success in CPT [19, 20] and double-resonance microcell-based clocks [21].

Instabilities of the clock frequency can also be induced by any evolution of the cell inner atmosphere through the buffer-gas induced temperature and pressure shift of the atomic transition [22]. Buffer gas permeation through the cell glass windows has been identified as a limitation process [23], especially when light buffer gas, as helium or neon, are used. Reduction of helium permeation for ultra-high vacuum (UHV)-cell-based applications has been achieved by employing

45 alumino-silicate glass (ASG) for the cell windows [24, 25]. However, to our knowledge, no
46 data has been reported demonstrating the benefits of ASG as an efficient permeation barrier for
47 microcells with other buffer gases.

48 In a previous study [20], we have undertaken the implementation of a CPT-based microcell atomic
49 clock using symmetric auto-balanced Ramsey (SABR) spectroscopy for light-shift mitigation.
50 Despite a reduction of the clock frequency sensitivity to light-field parameters by a factor higher
51 than 100 in comparison with the standard continuous-wave (CW) regime, the clock stability
52 remained limited for integration times higher than 1000 s by another mechanism, which we
53 attributed to Ne permeation through the cell borosilicate glass (BSG) windows.

54 In this paper, we report on the stability performance progress of this pulsed CPT-based microcell
55 atomic clock. The latter is not fully-integrated and uses an external acousto-optic modulator
56 (AOM) for generation of the pulsed optical sequence. The clock, based now on a Cs-Ne
57 microfabricated cell built with lower-permeation ASG windows, uses the SABR interrogation
58 technique, in conjunction with active servos of the setup temperature, the microwave power, and
59 the laser power. In this configuration, the clock Allan deviation reaches 1.4×10^{-12} at 10^5 s
60 integration time. This stability result at 1 day is an order of magnitude better than reported in [20]
61 and is competitive with those of best microwave clocks based on microcells [4, 14, 21].

62 2. Experimental set-up

63 Figure 1 describes the CPT clock experimental setup. This system was described in [20] and is
64 briefly reminded here. The clock transition of Cs atoms, confined in a microfabricated vapor
65 cell [26] filled with a pressure (~ 87 Torr) of Ne buffer gas, is probed by an optically-carried
66 9.192 GHz signal, obtained by direct current modulation at 4.596 GHz of a vertical-cavity
67 surface-emitting laser (VCSEL) [27]. The laser is tuned on the Cs D₁ line ($\lambda = 894.6$ nm)
68 and housed in a TO-46 package with integrated thermistance and Peltier element. The cell is
69 temperature-stabilized at 75°C. A static magnetic field of 23.4 μ T is applied to isolate the 0-0
70 clock transition. The cell is surrounded by a mu-metal magnetic shield to prevent magnetic
71 perturbations from the environment.

72 An acousto-optic modulator (AOM), placed at the laser output, is used to chop the light and then
73 produce the pulsed SABR interrogation sequence [20]. The latter is based on consecutive Ramsey
74 sequences with optical pulses of duration $T_b = 180 \mu$ s, followed either by a short dark time T_s of
75 100 μ s or a long dark time T_L of 250 μ s. The signal is detected at a time $\tau_d = 10 \mu$ s after the
76 pulse trigger during a detection window of length $\tau_D = 10 \mu$ s. A beam splitting cube is used
77 to collect a measurement of the laser power P_l at the cell input with a photodiode (PD1). The
78 circularly-polarized light beam, with a diameter of about 0.5 mm, is transmitted through the vapor
79 cell and detected by a second photodiode (PD2). The signal at the photodiode output is used in
80 several servo loops for stabilization of the laser and the local oscillator frequencies, as well as
81 for light-shift compensation. Optical sidebands that induce CPT resonance are connected to the
82 Cs atom $6^2P_{1/2}$, $F' = 4$ excited state. The microwave synthesizer that delivers the 4.596 GHz
83 signal is piloted by an active hydrogen maser used as a reference for frequency shifts and stability
84 measurements.

85 The experimental setup is implemented onto a table-top optical breadboard. The latter is
86 surrounded by a box with foam that provides passive temperature isolation. Two Schottky diodes
87 were placed between the microwave synthesizer output and the VCSEL input bias-tee. The first
88 one monitors the microwave power $P_{\mu W_i}$ of the incident 4.596 GHz signal at the synthesizer
89 output while the second one measures through a microwave circulator the microwave power $P_{\mu W_r}$
90 reflected by the VCSEL. In this study, the impact of a microwave power servo was investigated.
91 In this case, the microwave power $P_{\mu W_i}$, detected by one of the Schottky diodes, is converted
92 into a voltage signal and hence compared to an ultra-stable voltage reference. An error signal,
93 processed in a basic proportional-integral (PI) controller, is then used to correct the microwave

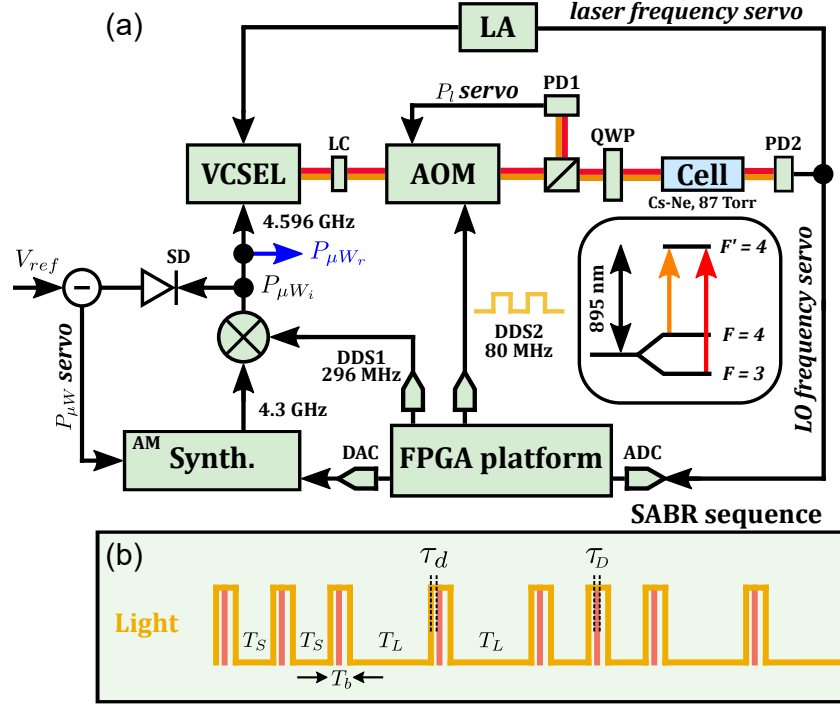


Fig. 1. (a): Schematic of the CPT clock experimental setup. A Cs vapor, diluted by a Ne buffer gas pressure in a microfabricated cell, interacts with optical CPT pulses generated with the help of a microwave-modulated VCSEL and an external AOM. AOM: acousto-optic modulator, SD: Schottky diode, QWP: quarter-wave plate, LA: lock-in amplifier, ADC: analog-to-digital converter, DAC: digital-to-analog converter, Synth.: microwave synthesizer. The inset shows the energy levels of the Cs atom involved in the CPT interaction. (b): Light pattern produced in the SABR sequence [20].

94 power delivered by the microwave synthesizer. A comparable system was used to investigate the
 95 impact of laser power stabilization. In this case, the voltage signal at the output of the photodiode
 96 PD1 is compared to a voltage reference to provide a correction signal sent to the power of the RF
 97 signal that drives the AOM.

98 3. MEMS cell with ASG windows and setup temperature control

99 In our previous study [20], we suspected that Ne permeation through the cell glass windows
 100 could limit the clock frequency stability for integration times higher than 1000 s. To validate
 101 this assumption, we have developed a new wafer of Cs-Ne cells using low-permeation ASG
 102 windows [24]. Both BSG and ASG cells use the same dispenser technology and were laser-
 103 activated with comparable parameters. In this work, the Ne pressure at 0°C of BSG and ASG
 104 cells is estimated from [22] to be 88 ± 2 Torr and 87 ± 2 Torr, respectively. The Ne pressure in
 105 the cell induces for both cells a clock frequency shift of about 50 kHz. We remind here that the
 106 pressure shift coefficient for Cs clock transition in the presence of Ne gas is positive (686 ± 14
 107 Hz/Torr) [22]. Thus, in our experiment, a leak of Ne gas leads to a progressive reduction of the
 108 clock frequency.

109 Figure 2 shows temporal traces of the clock frequency, recorded with the same experimental setup,
 110 but with two different Cs-Ne microcells, with windows made of BSG or ASG windows. The cell

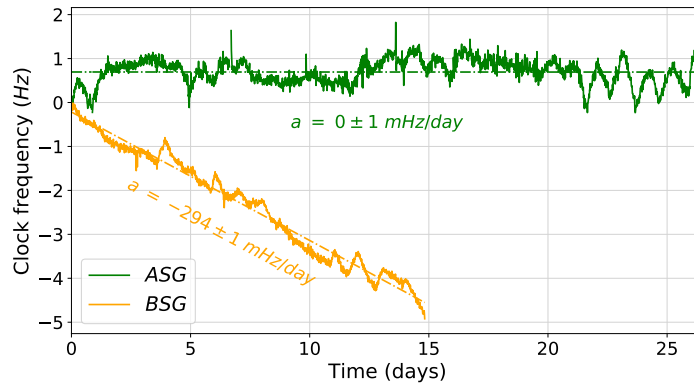


Fig. 2. Temporal trace of the clock frequency, using Cs-Ne microfabricated cells, having either BSG or ASG windows. For the ASG (BSG) cell, the 0 value on the y-axis corresponds to a central frequency of 9.192 682 333 (9.192 681 869) GHz. The initial clock frequency difference for the two cells is attributed to a slight difference of Ne pressure (~ 1 Torr).

111 with BSG windows leads to a negative clock frequency drift, assumed to be the signature of a Ne
 112 gas leak. The fitting of experimental data by a linear function yields a rate of -294 ± 1 mHz/day.
 113 This value is in good agreement with the clock frequency stability measured at 1 day when using
 114 a similar Cs-Ne cell heated at 70°C [20]. Fitting data by an exponential decay, we estimate the
 115 permeation rate for Neon through BSG to be about $3.3 \times 10^{-22} \text{ m}^2 \cdot \text{s}^{-1} \cdot \text{Pa}^{-1}$ at 75°C . Although
 116 this value is twice higher than the one reported in [28], it corresponds to the one extracted
 117 from a Cs-Ne clock frequency measurement performed at 81°C reported in [23]. With the cell
 118 having ASG windows, the clock is much more stable on the long-term. In this case, fitting of
 119 experimental data by a linear function gives a rate of 0 ± 1 mHz/day. These results strongly
 120 suggest that the use of ASG windows will mitigate the contribution of Ne gas permeation onto
 121 the clock long-term stability.

122 Despite the relevant improvement obtained with ASG, residual fluctuations of the clock
 123 frequency remain for shorter integration times, as it can be seen on Fig. 2. Looking at the

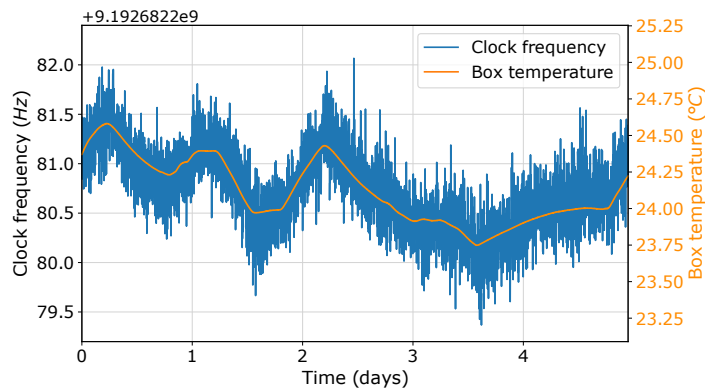


Fig. 3. Observed correlation between the clock frequency and the re-scaled setup box temperature. For information, the typical daily variations of the box temperature are 0.45°C . The maximum box temperature variations along the 5 days are 0.8°C .

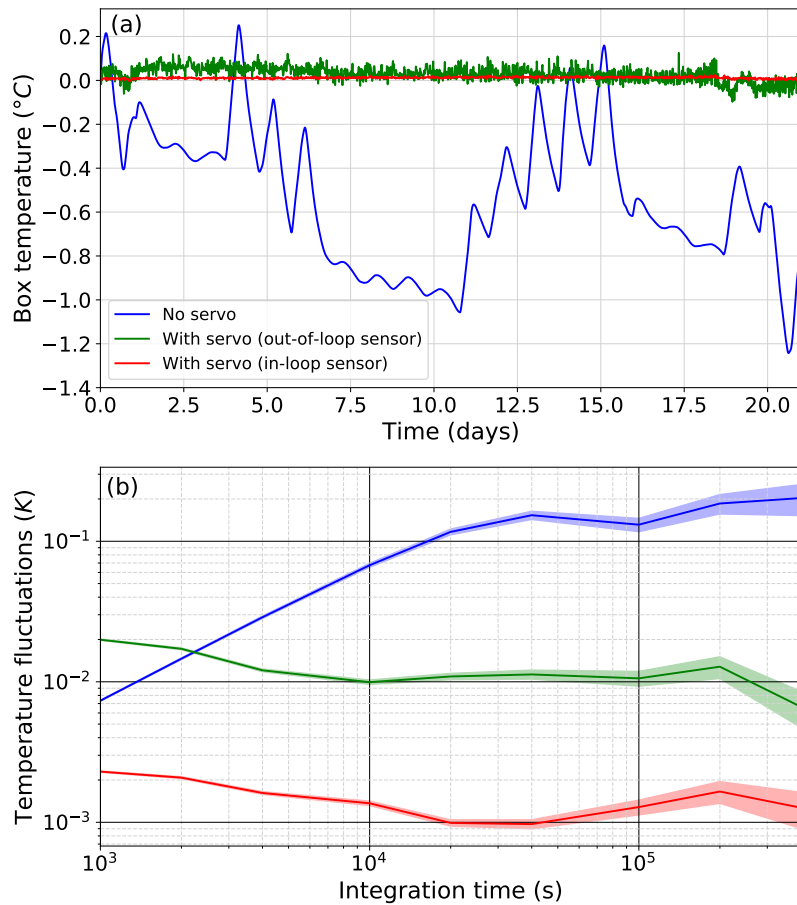


Fig. 4. (a) Temporal trace of the setup box temperature in normal and locked conditions. In the locked case, an in-loop and out-of-loop sensor are monitored. Offsets were applied to the temperatures for clarity. Temperatures at $t = 0$ are 26.2, 29.3 and 29°C for the "no servo", "with servo (out-of-loop)" and "with servo (in-loop)" cases, respectively. One point was kept every 1000 s. (b) Temperature fluctuations (K) of sensors, derived from data shown in (a), versus the integration time. The color code of Fig. 4(a) legend is kept. Colored zones indicate the size of error bars.

124 evolution of experimental parameters during the clock run, we found a clear correlation between
 125 the clock frequency and the setup box temperature variations. This behaviour is illustrated in
 126 Fig. 3 with another measurement data set of 5 days, where the box temperature was re-scaled,
 127 averaged for clarity and superimposed to the clock frequency data.

128 For better knowledge and control of the setup temperature, we have distributed over the setup
 129 breadboard 5 heating resistances and 7 thermistors. 6 sensors are used for monitoring while
 130 the seventh, placed between the quarter-wave plate and the CPT cell package, is used for the
 131 setup temperature control. The setup temperature in the box, measured at about 26°C (see Fig. 3
 132 and caption) before implementation of the servo, was tuned at the level of about 29°C with the
 133 servo (see Fig. 4 and caption). This temperature remains much lower than the one of some key
 134 components of the setup such as the laser and the cell.

135 Figure 4(a) shows a temporal trace of the setup box temperature, measured for more than
 136 20 days with an independent thermistor, with or without stabilization of the temperature. The

137 temperature of the thermistor used by the temperature controller (in-loop sensor) is also reported
 138 for information. An averaging window of 1000 s is used to plot these data. We observe that
 139 temperature variations of the setup are drastically mitigated when the lock is activated. For
 140 complimentary information, Fig. 4(b) shows typical temperature fluctuations, extracted from
 141 data shown in Fig. 4(a), of the respective sensors, in free-running and locked cases, versus the
 142 integration time. Temperature variations of the out-of-loop sensor are reduced by one order of
 143 magnitude at 10^5 s in the locked case, yielding residual temperature fluctuations of about 0.01 K.
 144 The in-loop sensor shows temperature fluctuations around 1 mK at 10^5 s.

145 4. Clock frequency stability progress

146 This section reports on the evaluation progress of the clock fractional frequency stability. It aims
 147 to demonstrate how the clock stability was improved by progressively implementing additional
 148 servos of the setup box temperature, the microwave power and the laser power.

149 Figure 5 shows the clock Allan deviation recorded with the ASG cell, with or without stabilization
 150 of the setup box temperature. Microwave and power servos are not activated. The laser power P_l
 151 is $100 \mu\text{W}$ and the microwave power $P_{\mu W_i}$ is -0.49 dBm (0.89 mW). The blue curve of Fig. 5
 152 shows results obtained without temperature stabilization of the setup box. In this case, the clock
 153 stability is limited at the level of about 10^{-11} at 10^5 s. When the setup temperature is stabilized
 154 (green curve), the clock Allan deviation is measured to be 1.5×10^{-10} at 1 s, 3.8×10^{-12} at 10^5 s
 155 and below 10^{-11} at 3×10^5 s. The clock stability at 1 day integration time is about one order of
 156 magnitude better than the one reported in [20], and is found in good agreement with the Allan
 157 deviation calculated from data shown in Fig. 3, where both the effect of the setup temperature
 158 and a residual linear drift (corresponding to permeation), would be subtracted from the raw data.

159 During clock operation, we have monitored some key experimental parameters in order to
 160 identify the new main contributions to the clock mid-term stability. In Fig. 5, the red curve depicts
 161 the contribution to the Allan deviation of the microwave power fluctuations. This contribution
 162 is derived from voltage fluctuations ΔV recorded at the output of the Schottky diode ($\Delta V/V =$
 163 7.2×10^{-4} at 10^5 s) and includes fictitious input microwave power fluctuations induced by the
 164 temperature sensitivity of the Schottky diode power-to-voltage coefficient. With a measured
 165 dependence of the clock frequency to microwave power variations of 4.7×10^{-12} (in fractional
 166 value), this contribution reaches $3\text{-}4 \times 10^{-12}$ at 10^5 s, a level comparable to the clock Allan

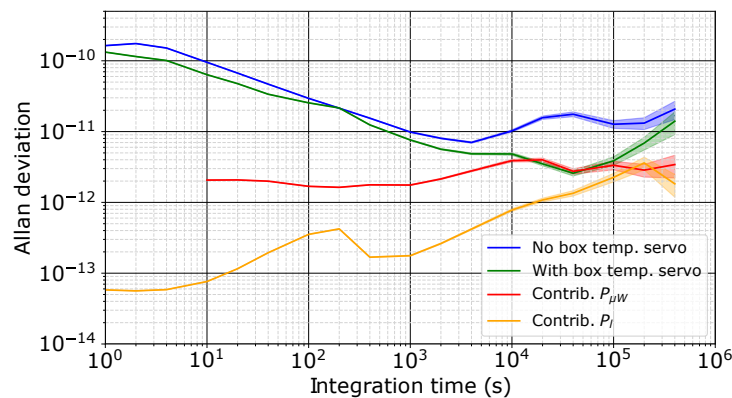


Fig. 5. Allan deviation of the clock frequency, with or without temperature stabilization of the setup breadboard. Contributions of the laser power and microwave power fluctuations to the clock Allan deviation are also shown. Colored zones indicate the size of error bars.

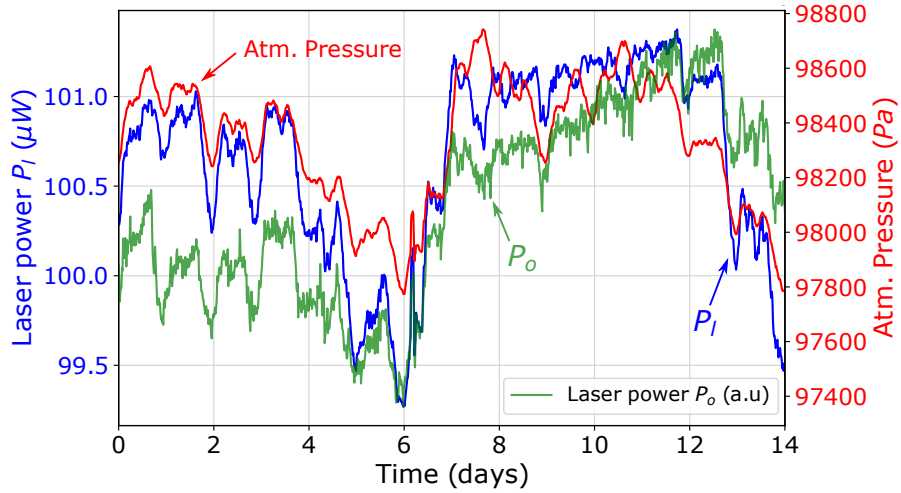


Fig. 6. Observed correlation between the atmospheric pressure, P_I the laser power at the cell input (PD1) and P_O the laser power at the cell output, measured in clock operation (PD2).

167 deviation result.

168 The second contribution to the clock stability, depicted by the orange curve in Fig. 5, is the
 169 contribution of laser power fluctuations. Here, laser power fluctuations at the cell input, obtained
 170 by measuring the laser power detected by the photodiode PD1 and adequate calibration, are
 171 multiplied by the sensitivity coefficient of the clock frequency versus laser power dependence
 172 curve ($6.5 \times 10^{-12}/\mu\text{W}$ in fractional value). With fractional laser power fluctuations $\Delta P_I/P_I \approx 3$
 173 $\times 10^{-3}$ at 10^5 s ($\Delta P_I \approx 0.3 \mu\text{W}$), we obtain that laser power fluctuations limit the clock stability
 174 at the level of about 2×10^{-12} at 10^5 s.

175 As shown in Fig. 6, we have noticed that the laser power P_I measured at the cell input (photodiode
 176 PD1), and consequently the laser power P_O at the cell output (PD2), were correlated with the
 177 atmospheric pressure measured in the lab. This can be explained by the fact that the VCSEL
 178 package used in this setup is not vacuum-sealed and then not immune to ambient pressure
 179 variations. Over a measurement of 6 days, we have also observed, without microwave power
 180 stabilization, that both microwave power signals, $P_{\mu W_i}$ and $P_{\mu W_r}$, showed periodically some
 181 spikes, also visible on the laboratory temperature data. This observation is consistent with the fact
 182 that some microwave components and detectors were initially out of the temperature-controlled
 183 setup box, experiencing ambient temperature fluctuations.

184 For further mitigation of light-shifts contributions, we have first envisioned to reduce the
 185 microwave power contribution shown in Fig. 5 (red curve). In this process, we studied the impact
 186 of the temperature dependence of the Schottky diode power-to-voltage coefficient. At fixed input
 187 microwave power, we measured that the voltage output of the Schottky diode could change at the
 188 level of -8×10^{-5} V/K. Given our experimental conditions, we calculated then that a variation
 189 of 1 K of the Schottky diode could induce, in closed-loop configuration of a microwave power
 190 servo, a clock frequency variation of $1.3 \times 10^{-11}/\text{K}$ (in fractional value). With the Schottky
 191 diode out of the box and considering that 0.3 K temperature variation can be experienced within
 192 the experimental room, this sensitivity could have limited the clock stability at 10^5 s at the level
 193 of about 4×10^{-12} , comparable to the clock Allan deviation (green curve) of Fig. 5.

194 We placed first the Schottky diode into the temperature stabilized box, without microwave power
 195 servo. In this configuration, the contribution of the microwave power at 10^5 s, treated as in Fig.

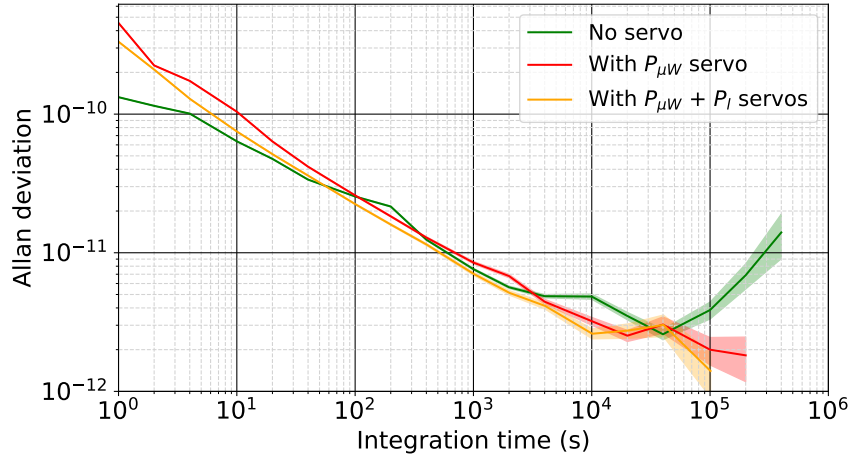


Fig. 7. Allan deviation of the clock frequency, with stabilization of the setup box temperature, in different configurations: no additional servos, with only microwave power servo, with microwave and laser power servo. Colored zones indicate the size of error bars.

196 5, was found to be comparable with the one measured in Fig. 5.

197 We have then implemented a microwave power servo, with the Schottky diode in the box. This
 198 test was performed with a comparable laser power $P_l \approx 100 \mu\text{W}$ and a microwave power $P_{\mu W}$
 199 $\approx 0.82 \text{ mW}$. With this servo, microwave power fluctuations $\Delta P_{\mu W}/P_{\mu W}$, measured through
 200 the in-loop Schottky diode, were reduced at 1 day by almost an order of magnitude, reaching
 201 9.7×10^{-5} ($\Delta P_{\mu W} \approx 81 \text{ nW}$ at 1 day). With this number, the contribution of the microwave
 202 power variations to the clock stability would be rejected at the level of 3.8×10^{-13} at 10^5 s .
 203 With this servo, the clock frequency stability was improved, as shown in Fig. 7, at the level of
 204 2×10^{-12} at 10^5 s and slightly below 2×10^{-12} at $2 \times 10^5 \text{ s}$.

205 This level being comparable to the laser power contribution indicated in Fig. 5, we have
 206 performed a last stability test by adding the laser power servo. In this test, the laser power
 207 P_l was $75 \mu\text{W}$ while the microwave power was 0.73 mW . Using this servo, fractional laser
 208 power fluctuations $\Delta P_l/P_l$, extracted from the in-loop sensor (PD1), were reduced at the level of
 209 4.1×10^{-5} ($\Delta P_l \approx 3 \text{ nW}$) at 10^5 s . In this configuration, the clock Allan deviation, extracted
 210 from a shorter measurement (5 days) and given the confidence intervals, is comparable or very
 211 slightly improved at a level below 2×10^{-12} at 10^5 s .

212 5. Conclusions

213 We have reported the progress of a table-top CPT-based Cs atomic clock using a symmetric
 214 auto-balanced Ramsey (SABR) interrogation technique and a microfabricated cell, filled with
 215 Neon, with low permeation ASG windows. We demonstrated that ASG reduces significantly Ne
 216 permeation through the cell glass in comparison with standard borosilicate glass (BSG). This
 217 solution allows to mitigate the impact of the cell atmosphere evolution to the clock mid- and
 218 long-term stability. Since light-shift effects remained the main contribution to the clock stability
 219 for $\tau > 10^4 \text{ s}$, we implemented active stabilization of the setup box temperature, microwave power
 220 and laser power. The addition of these servos contributed to yield a clock Allan deviation of $1.4 \times$
 221 10^{-12} at 10^5 s . These results at 1 day, competitive with those of best microwave microcell-based
 222 atomic clocks [4, 14, 21], are more than 10 times better than obtained previously with this clock
 223 demonstrator [20]. In the future, the implementation of the pulsed SABR sequence without

224 the use of an external AOM will be investigated. Several approaches might be explored for
225 this purpose [29–31]. This might pave the way to the advent of new-generation fully-integrated
226 pulsed CPT atomic clocks with enhanced stability.

227 **Funding.** C. Carlé’s PhD thesis is co-funded by CNES (Centre National d’Etudes Spatiales) and AID
228 (Agence Innovation Défense). This work was supported in part by DGA (Direction Générale de l’Armement),
229 in part by Région de Franche-Comté, and in part by Agence Nationale de la Recherche (ANR) in the frame
230 of the LabeX FIRST-TF (Grant No. ANR 10-LABX-0048), EquipX Oscillator-IMP (Grant No. ANR
231 11-EQPX-0033) and ASTRID PULSACION (Grant No. ANR-19-ASTR-0013-01) projects. This work was
232 also partially supported by the French RENATECH network and its FEMTO-ST technological facility.

233 **Disclosures.** The authors declare no conflicts of interest.

234 **Data availability.** Data underlying the results presented in this paper are not publicly available at this time
235 but may be obtained from the authors upon reasonable request.

236 References

- 237 1. S. Knappe, V. Shah, P.D.D. Schwindt, L. Hollberg, L.-A. Liew and J. Moreland, “A microfabricated atomic clock,”
238 *Appl. Phys. Lett.* **85**, 9, 1460–1462 (2004).
- 239 2. S. Knappe, “MEMS atomic clocks,” in *Compr. Microsystems*, Y. B. Gianchandani, O. Tabata and H. Zappe, ed.,
240 (Elsevier, 2008), pp 571–612.
- 241 3. J. Kitching, “Chip-scale atomic devices,” *Appl. Phys. Rev.* **5**, 031302 (2018).
- 242 4. H. Zhang, H. Hans, N. Tharayil, A. Shirane, M. Suzuki, K. Harasaka, K. Adachi, S. Goka, S. Yanagimachi, K. Okada,
243 “ULPAC: A miniaturized ultra-low-power atomic clock,” *IEEE Journ. Solid State Circuits* **54**, 11, 3135–3148 (2019).
- 244 5. R. Lutwak, A. Rashed, M. Varghese, G. Tepolt, J. LeBlanc, M. J. Mescher, D. K. Serkland, K. M. Geib, G. M. Peake,
245 S. Römisch “The Chip-Scale Atomic Clock-Prototype Evaluation,” *Proc. 39th Annu. Precise Time Interval*
246 *(PTTI) Meet.*, (The Institute of Navigation, 2007), pp. 269–290.
- 247 6. R. Lutwak, A. Rashed, M. Varghese, G. Tepolt, J. LeBlanc, M. J. Mescher, D. K. Serkland, G. M. Peake, “The
248 Miniature Atomic Clock - Pre-Production Results,” *Proc. IEEE Int. Freq. Control. Symp. - Eur. Freq. Time Forum Jt.*
249 *Meet.*, (IEEE, 2007), pp. 1237–1333.
- 250 7. J. Vanier, “Atomic clocks based on coherent population trapping: a review,” *Appl. Phys. B* **81**, 4, 421–442 (2005).
- 251 8. M. Zhu and L. S. Cutler, “Theoretical and experimental study of light shift in a CPT-based Rb vapor cell frequency
252 standard,” *Proc. 32nd Annu. Precise Time Interval (PTTI) Meet.*, (The Institute of Navigation, 2000), pp.
253 311–323.
- 254 9. V. Shah, V. Gerginov, P. D. D. Schwindt, S. Knappe, L. Hollberg and John Kitching, “Continuous light-shift correction
255 in modulated coherent population trapping clocks,” *Appl. Phys. Lett.* **89**, 151124 (2006).
- 256 10. B. H. McGuyer, Y.-Y. and W. Happer, “Simple method of light-shift suppression in optical pumping systems,” *Appl.*
257 *Phys. Lett.* **94**, 251110 (2009).
- 258 11. Y. Zhang, W. Yang, S. Zhang and J. Zhao, “Rubidium chip-scale atomic clock with improved long-term stability
259 through light intensity optimization and compensation for laser frequency detunings,” *J. Opt. Soc. Am. B* **33**, 8,
260 1756–1763 (2016).
- 261 12. D. Miletic, C. Affolderbach, M. Hasegawa, R. Boudot, C. Gorecki and G. Miletic, “AC Stark-shift in CPT-based Cs
262 miniature atomic clocks,” *Appl. Phys. B* **109**, 8, 89-97 (2012).
- 263 13. R. Vicarini, M. Abdel Hafiz, V. Maurice, N. Passilly, E. Kroemer, L. Ribetto, V. Gaff, C. Gorecki, S. Galliou and R.
264 Boudot, “Mitigation of temperature-induced light-shift effects in miniaturized atomic clocks,” *IEEE Trans. Ultrason.*
265 *Ferroelec. Freq. Contr.* **66**, 12, 1962–1967 (2019).
- 266 14. S. Yanagimachi, S. Harasaka, R. Suzuki, M. Suzuki and S. Goka, “Reducing frequency drift caused by light shift in
267 coherent population trapping-based low-power atomic clocks,” *Appl. Phys. Lett.* **116**, 104102 (2020).
- 268 15. V. Yudin, M. Yu. Basalaev, A. V. Taichenachev, J. W. Pollock, Z. L. Newman, M. Shuker, A. Hansen, M. T. Hummon,
269 R. Boudot, E. A. Donley and J. Kitching, “General methods for suppressing the light-shift in atomic clocks using
270 power modulation,” *Phys. Rev. Appl.* **14**, 024001 (2020).
- 271 16. M. Abdel Hafiz, R. Vicarini, N. Passilly, C. E. Calosso, V. Maurice, J. Pollock, A. Taichenachev, V. I. Yudin, J.
272 Kitching and R. Boudot, “Protocol for light-shift compensation in a continuous-wave microcell atomic clock,” *Phys.*
273 *Rev. Appl.* **14**, 034015 (2020).
- 274 17. S. Micalizio, C. E. Calosso, A. Godone and F. Levi, “Metrological characterization of the pulsed Rb clock with
275 optical detection,” *Metrologia* **49**, 425-436 (2012).
- 276 18. M. Abdel Hafiz, G. Coget, M. Petersen, C. E. Calosso, S. Guérandel, E. de Clercq and R. Boudot, “Symmetric
277 autobalanced Ramsey interrogation for high-performance coherent population-trapping vapor-cell atomic clock,”
278 *Appl. Phys. Lett.* **112**, 244102 (2018).
- 279 19. C. Carlé, M. Petersen, N. Passilly, M. Abdel Hafiz, E. de Clercq and R. Boudot, “Exploring the use of Ramsey-CPT
280 spectroscopy for a microcell-based atomic clock,” *IEEE Trans. Ultrason. Ferroelec. Freq. Contr.* **68**, 10, 3249–3256
281 (2021).

- 282 20. M. Abdel Hafiz, C. Carlé, N. Passilly, J.-M. Danet, C. E. Calosso and Rodolphe Boudot, "Light-shift mitigation in a
283 microcell-based atomic clock with symmetric auto-balanced Ramsey spectroscopy," *Appl. Phys. Lett.* **120**, 064101
284 (2022).
- 285 21. E. Batori, C. Affolderbach, M. Pellaton, F. Gruet, M. Violetti, Y. Su, A. K. Skrivervik and G. Mileti, " μ POP clock: A
286 microcell atomic clock based on a double-resonance Ramsey scheme," *Phys. Rev. Appl.* **18**, 054039 (2022).
- 287 22. O. Kozlova and S. Guérandel and E. de Clercq, "Temperature and pressure shift of the Cs clock transition in the
288 presence of buffer gases: Ne, N₂, Ar," *Phys. Rev. A* **83**, 062714 (2011).
- 289 23. S. Abdullah, C. Affolderbach, F. Gruet and G. Mileti, "Aging studies on micro-fabricated alkali buffer-gas cells for
290 miniature atomic clocks," *Appl. Phys. Lett.* **106**, 163505 (2015).
- 291 24. A. T. Dellis and V. Shah and E. A. Donley and S. Knappe and J. Kitching, "Low helium permeation cells for atomic
292 microsystems technology," *Opt. Lett.* **41**, 12, 2775–2778 (2016).
- 293 25. J. P. McGilligan and K. R. Moore and A. Dellis and G. D. Martinez and E. de Clercq and P. F. Griffin and A. S.
294 Arnold and E. Riis and R. Boudot and J. Kitching, "Laser cooling in a chip-scale platform," *Appl. Phys. Lett.* **117**,
295 054001 (2020).
- 296 26. R. Vicarini, V. Maurice, M. Abdel Hafiz, J. Rutkowski, C. Gorecki, N. Passilly, L. Ribetto, V. Gaff, V. Volant, S.
297 Galliou and R. Boudot, "Demonstration of the mass-producible feature of a Cs vapor microcell technology for
298 miniature atomic clocks," *Sens. Actuat. A: Phys.* **280**, 99-106 (2018).
- 299 27. E. Kroemer, J. Rutkowski, V. Maurice, R. Vicarini, M. Abdel Hafiz, C. Gorecki, and R. Boudot, "Characterization of
300 commercially available vertical-cavity surface-emitting lasers tuned on Cs D₁ line at 894.6 nm for miniature atomic
301 clocks," *Appl. Opt.* **55**, 31, 8839–8847 (2016).
- 302 28. J. Shelby, "Helium, deuterium, and neon migration in a common borosilicate glass," *J. Appl. Phys.* **45**, 5, 2146–2149
303 (1974).
- 304 29. T. Ide, S. Goka and Y. Yano, "CPT pulse excitation method based on VCSEL current modulation for miniature atomic
305 clocks," *Proc. IEEE Int. Freq. Control. Symp. - Eur. Freq. Time Forum Jt. Meet.*, (IEEE, 2015), pp. 269–290.
- 306 30. J. Yang, Y. Tian, B. Tan, P. Yun and S. Gu, "Exploring Ramsey-coherent population trapping atomic clock realized
307 with pulsed microwave modulator laser," *J. Appl. Phys.* **115**, 093109 (2014).
- 308 31. M. Jafati, I. J. Guo and M. Rais-Zadeh, "An ultra-fast optical shutter exploiting total light absorption in a phase
309 change material," *Proc. SPIE* **10000**, 101000I (2017).